

# Instability of plasma plume of micro-hollow cathode discharge

D. Levko,<sup>1</sup> Y. P. Bliokh,<sup>2</sup> V. Tz. Gurovich,<sup>2</sup> and Ya. E. Krasik<sup>2</sup>

<sup>1</sup>Department of Aerospace Engineering and Engineering Mechanics, The University of Texas at Austin, Austin, Texas 78712, USA

<sup>2</sup>Department of Physics, Technion, 32000 Haifa, Israel

(Received 29 September 2015; accepted 21 October 2015; published online 3 November 2015)

The micro-hollow cathode gas discharge driven by thermionic emission is studied using the two-dimensional particle-in-cell Monte Carlo collisions simulation. The electron current is extracted from the plasma plume penetrating into the keeper–anode space through a small keeper orifice from the cathode–keeper space. The results of simulations and a simplified analytical model showed that the plasma density and extracted current can exhibit deep modulation in the range of frequencies of tens of MHz. This modulation appears when the space-charge limited current between the plume boundary and the anode exceeds the plasma thermal electron current through the orifice.

© 2015 AIP Publishing LLC. [<http://dx.doi.org/10.1063/1.4935116>]

## I. INTRODUCTION

Recent trends in space propulsion are associated with the paradigm shift toward small and efficient satellites or micro-satellites.<sup>1</sup> These satellites require a rather small thrust for their position control. The thrust is generated by a beam of positive ions ejected by ion and Hall plasma thrusters.<sup>2</sup> In order to produce the plasma in these thrusters and to prevent the satellite charging because of the positive charge of the ejected ion beam, electron beams generated by hollow cathodes are efficiently used.<sup>2,3</sup>

Small thrusters produce low-current ion beams. The neutralization of this current requires also a rather small electron current, which can be produced by miniature micro-hollow cathodes (mHC).<sup>4–8</sup> Because of their small dimensions, the experimental investigation of mHCs is problematic. Therefore, various numerical simulations (particle-in-cell and fluid) are useful.<sup>9–12</sup>

In outer space, HCs operate with highly non-uniform neutral gas density.<sup>2</sup> That is, the gas density is the largest inside the emitter–keeper (E-K) space and decreases rapidly outside the keeper. Such a distribution of neutral gas density may induce different instabilities, which were discovered in both Hall thrusters<sup>13</sup> and hollow cathodes.<sup>9,10,14</sup> For instance, as shown in Ref. 10, the ion acoustic turbulence is responsible for the generation of energetic ions in the plasma plume, which leads to the keeper electrode being quickly damaged.

In the present paper, we report another possible mechanism of mHC instability. This instability arises in the keeper–anode (K-A) gap and is explained by the electron and ion dynamics in the plasma plume.

## II. RESULTS AND DISCUSSION

### A. Geometry and parameters

The details of the two-dimensional self-consistent particle-in-cell Monte Carlo collisions (2D PIC/MCC) model that is used in the present research were given in earlier publications.<sup>11</sup> The model is based on the 2D Cartesian module of the open-source WARP PIC code.<sup>15</sup> The plasma consists

of electrons, ions  $Xe^+$ , and neutral  $Xe$  atoms. In order to decrease the simulation time, the ion mass is taken equal to 1 amu.

The 2D simulation domain is shown in Fig. 1(a). The domain consists of three coaxial electrodes, namely, a hollow emitter, keeper, and anode. The keeper with a small diameter orifice protects the emitter from bombardment by energetic ions that can be accelerated from the plasma existing in the K-A space. In addition, to prevent the energetic ions interacting with the emitter, the latter is shielded by a plate, the orifice of which has a diameter smaller than the inner diameter of the emitter and keeper orifice. The electrons are emitted from the inner surface of the emitter because of thermionic emission. The latter is described by the Richardson-Dushman equation accounting for the Schottky effect.<sup>2</sup>

The inner and the outer emitter radii are  $50\ \mu\text{m}$  and  $85\ \mu\text{m}$ , respectively, the emitter length is  $300\ \mu\text{m}$ , and the keeper inner radius, length, and the orifice radius are  $100\ \mu\text{m}$ ,  $410\ \mu\text{m}$ , and  $40\ \mu\text{m}$ , respectively. The distance between the outer boundary of the keeper and anode is  $270\ \mu\text{m}$ . The radius of the emitter plate orifice is  $35\ \mu\text{m}$ . These dimensions correspond to the mHC setup studied in Ref. 5.

Note that the results of simulations have shown that, for the considered geometry, gas density, and emitter temperature, the discharge is not ignited if the E-K voltage is below 40 V. Thus, the emitter and keeper potentials were considered to be  $-100\ \text{V}$  and  $-60\ \text{V}$ , respectively, and constant in time. In the simulation, it was assumed that the gas temperature is equal to the emitter temperature of 1500 K. The neutral gas density is defined using the model described in Ref. 16. In accordance with this model, the neutral gas density is almost constant inside the emitter and E-K gap and decreases as  $\sim 1/r^2$  outside the keeper, where  $r$  is the distance with respect to the output of the keeper orifice. The gas pressure inside the keeper is considered to be  $10^3\ \text{Pa}$ . Thus, the neutral gas density inside the keeper, at the outlet of the keeper's orifice, and near the anode is  $4.8 \times 10^{22}\ \text{m}^{-3}$ ,  $4.3 \times 10^{22}\ \text{m}^{-3}$ , and  $3.0 \times 10^{20}\ \text{m}^{-3}$ , accordingly. For these conditions, the

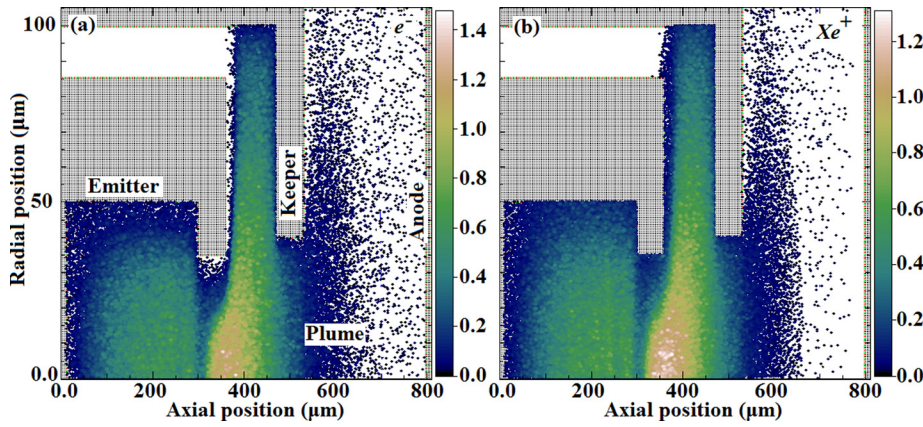


FIG. 1. Typical distribution of electron (a) and ion (b) density (at time  $t = 13.4$  ns with respect to the beginning of the discharge between the emitter and keeper). Plasma species densities should be multiplied by a factor of  $10^{20} \text{ m}^{-3}$ .

electron mean free path in the K-A gap is much larger than its length.

Figure 1 shows typical 2D snapshots of the electron and ion density distributions obtained as a result of PIC simulations. One can see that the density of the plasma inside the keeper is vastly larger than that in the K-A gap, which is the plasma plume.<sup>2</sup>

## B. Numerical results and analysis

Numerical simulation shows that the electron current extracted through the keeper orifice and collected by the anode experiences strong automodulation with frequency in the range of tens of MHz (see Fig. 2).

Let us consider the simple physical model, which explains the origin of this phenomenon. When the keeper orifice is filled by plasma, the penetration of the electric field from the K-A gap into the E-K region is insignificant. Thus, the discharge in the E-K gap can be assumed to be self-sustained in the sense that its parameters are independent of the K-A potential difference. This discharge can be considered as a source of the plasma that penetrates through the keeper orifice into K-A gap forming the plasma plume. The latter propagates toward the anode with ion sound velocity  $c_s = v_0 \sqrt{m/M}$ . Here,  $v_0$  is the average velocity of electrons in the plasma plume, and  $m$  and  $M$  are the electron and ion mass, respectively. The boundary of the plasma plume is the source of electrons extracted from the plasma and accelerated toward the anode by the electric field in the K-A gap.

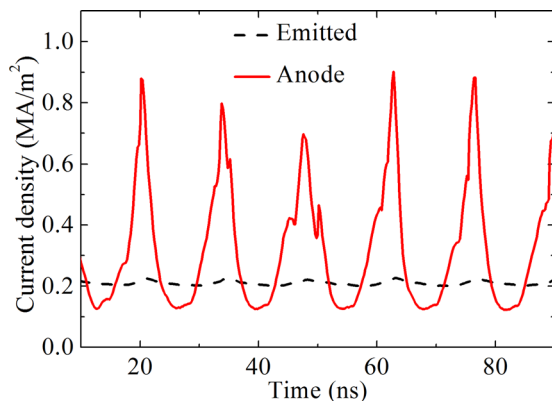


FIG. 2. Automodulation of the anode (solid curve) and emitted (dashed curve) electron current densities.

The electric field is screened in the plasma until the space-charge limited current of the extracted electrons is smaller than the current of the thermal electrons supplied by the plasma in the keeper orifice.

For a description of the processes in the plasma plume, let us consider a simplified one-dimensional model, assuming uniform plasma density distribution in the transversal direction. The solution of the Poisson equation, equation of the electron motion, and continuity equation allows one to obtain the potential distribution between the plasma plume boundary and the anode. The zero electric field at the plasma boundary (electron space-charge limited emission), the given value of the potential difference in the plasma boundary–anode gap, and the initial velocity  $v_0$  of the electrons extracted from the plasma constitute the boundary conditions. Omitting straightforward calculations, the extracted electron current density is described by the following expression:<sup>17</sup>

$$j = \frac{mv_0^3}{18\pi d^2} (\sqrt{\psi} - 1) (2 + \sqrt{\psi})^2, \quad (1)$$

where  $\psi = 2e\phi_0/mv_0^2$ ,  $\phi_0$  is the difference between the anode and plasma potentials, and  $d$  is the distance between the anode and the plasma plume boundary.

As the plasma propagates toward the anode, the distance  $d$  decreases and the current density increases as  $j \propto d^{-2}$ . However, the total electron current  $I = jS_p$ , where  $S_p$  is the effective area of the plasma boundary, that can be extracted from the plasma is limited by the current  $I_{max}$  of the electrons penetrating through the keeper orifice into the K-A gap. Thus, Eq. (1) is valid only when  $I \ll I_{crit} = 0.5en_p v_0 S$ , where  $n_p$  is the plasma density at the output of the keeper orifice, and  $S$  is the orifice cross-section area. Thus, Eq. (1) holds until

$$j < j_{crit} = 0.5en_p v_0 (S/S_p). \quad (2)$$

When the distance  $d$  becomes so small that the inequality (2) is violated, the electric field penetrates the plasma. This leads to the plasma ion flow toward the anode slowing down and the formation of a backward ion flow. As a result, a region with a non-compensated positive charge of ions is formed. A part of the slow plasma electrons are trapped by the potential well formed by these ions. Other, un-trapped, electrons leave the K-A gap, thus increasing the anode

current amplitude. Note that, because of the smallness of the orifice radius and the large difference between the plasma densities in the E-K and K-A spaces, the density of the plasma penetrating through the orifice practically does not depend on the value of the electron current extracted from the plasma boundary. When the ions leave the K-A space, the evolution of the plasma plume described above is repeated.

**C. Comparison with the results of PIC simulation**

When condition  $j < j_{crit}$  is satisfied, the value of the potential  $\varphi(z)$  is constant inside the plasma plume and increases linearly in the gap between the anode and the plasma boundary, as shown in Fig. 3. One can see that earlier in time, when  $j < j_{crit}$ , the plasma boundary moves toward the anode with an approximately constant velocity  $c_S \approx (2-2.5) \times 10^4$  m/s, which corresponds to  $v_0 \approx (0.86-1.07) \times 10^6$  m/s. Both these values,  $c_S$  and  $v_0$ , are in good agreement with the distributions of the electron and ion velocities in the A-K gap, which are shown, for example, in Fig. 4.

The slowing of the plasma boundary velocity (Fig. 3) indicates that the distance  $d$  becomes so small that the electron current density  $j$  approaches its critical value  $j_{crit}$ .

Now, using Eq. (1) and the positions of the plasma boundary versus the time, one can calculate the current density  $j(t)$  and compare it with the results of the numerical simulation. The results of this comparison are shown in Fig. 5. One can see a good agreement between the evolution of the current density obtained in the numerical simulation and the evolution described by Eq. (1). This indicates that the proposed simplified model describes adequately the underlying physics of the plasma plume instability.

The results of numerical simulations showed that the plasma density at the output of the keeper orifice is  $\sim 1.5 \times 10^{19} \text{ m}^{-3}$  (Fig. 1), so that  $j_{crit} \approx (0.36-0.45) \text{ MA/m}^2$  (shaded area in Fig. 5). When the electron current density exceeds this threshold value, the flux of electrons leaking through the orifice is insufficient to compensate the positive

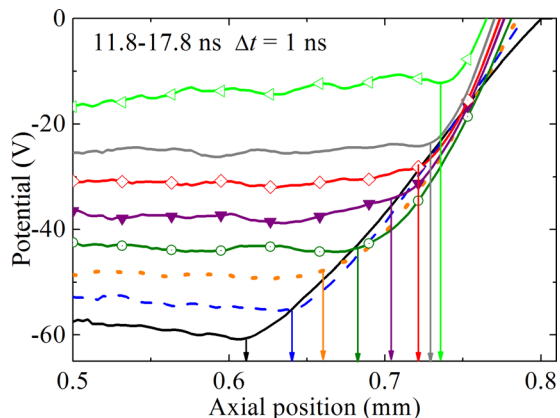


FIG. 3. Axial distribution of the potential  $\varphi(z)$  in the K-A gap. Distributions for different times (the time step is 1 ns) are shifted in the vertical direction to provide better visualization. The positions of the plasma boundary  $z_b(t)$  (marked by arrows) are defined as a coordinate where the potential  $\varphi(z)$  starts to grow.

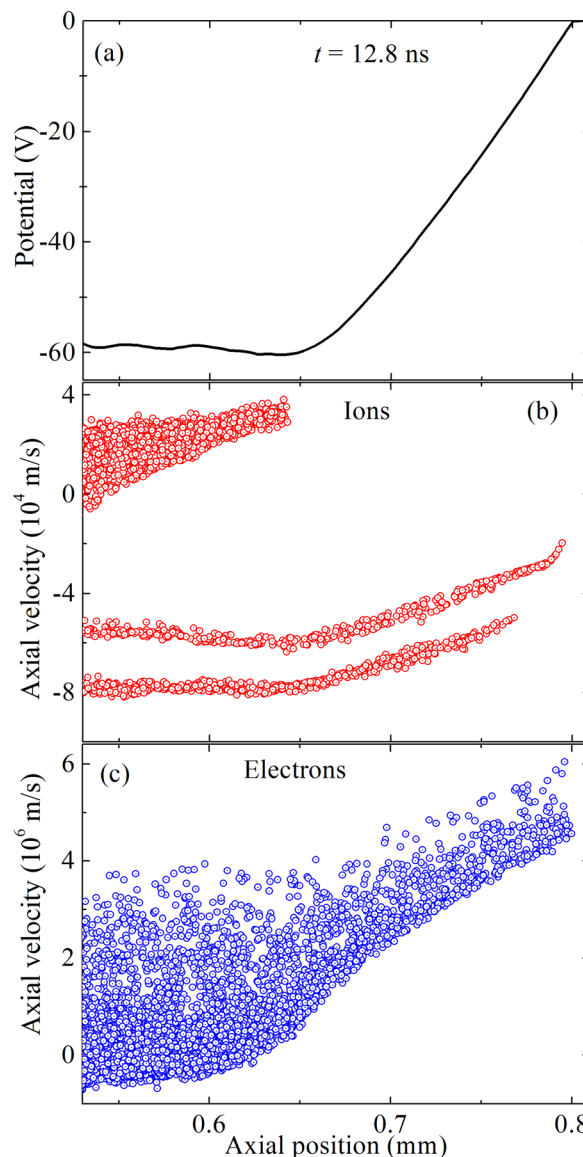


FIG. 4. (a) Axial distribution of the potential in the K-A gap. Phase space  $v_z(z)$  of ions (b) and electrons (c).

charge of ions in the K-A space and the electric field penetrates the plasma. Ions are slowed down and start moving backward to the keeper. As a result, a region with an

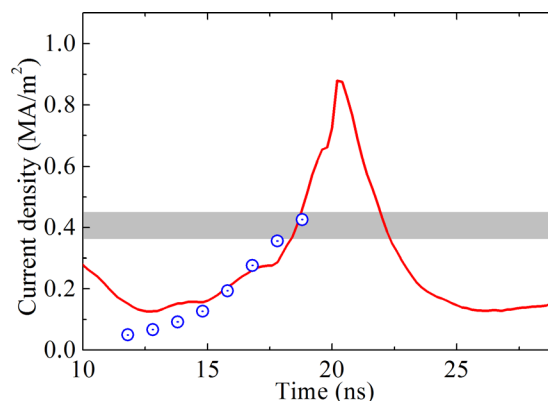


FIG. 5. Dependence of the electron current density versus time. Solid curve, numerical simulation; circles, Eq. (1). The shaded area marks the estimated value of  $j_{crit}$ .

enhanced positive space charge appears. This modifies strongly the axial distribution of the potential inside the space-charge non-compensated plasma, as shown in Fig. 6(a). The formation of the counter flow of ions is visible in Fig. 6(b), where the electron and ion phase spaces at  $t = 19.2$  ns are presented. Part of the plasma electrons are trapped in the potential well formed by the excess of the positive ion charge. These trapped electrons are clearly visible as a vortex in Fig. 6(c).

A strong violation of the plasma quasi-neutrality results in the penetration of the electric field into the plasma plume. The electric field, which appears near the output of the keeper orifice [see Fig. 7(a)], increases the electron flow extracted from the discharge plasma. This leads to an increase in the total electron current density toward the anode, which exceeds significantly its critical value  $j_{crit}$ . Simultaneously, the ions start leaving the A-K gap.

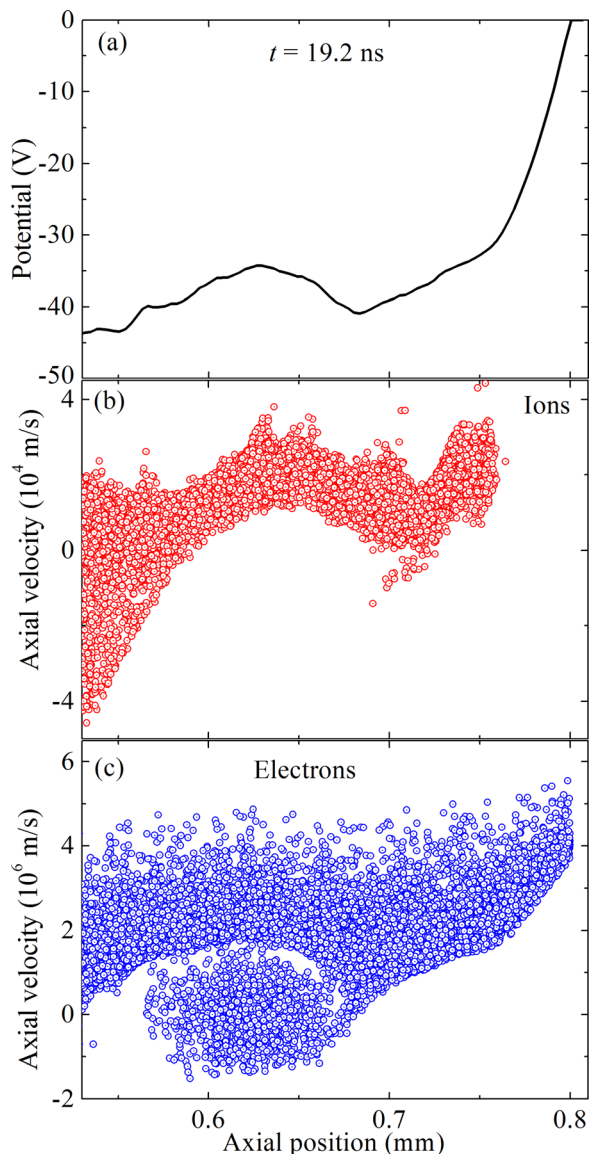


FIG. 6. Axial distribution of the potential  $\phi(z)$  (a) and phase space  $v_z(z)$  of ions (b) and electrons (c), when current density  $j$  exceeds the critical value  $j_{crit}$ ;  $t = 19.2$  ns.

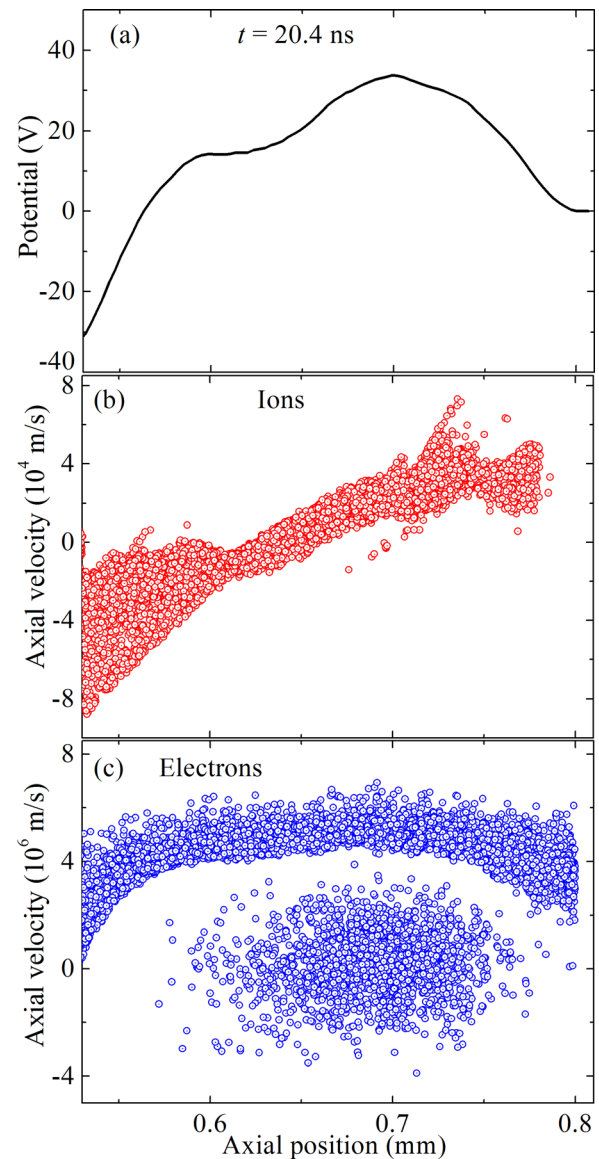


FIG. 7. Axial distribution of the potential  $\phi(z)$  (a) and phase space  $v_z(z)$  of ions (b) and electrons (c) when the current density reaches its maximum;  $t = 20.4$  ns. Note the appearance of the electric field near the orifice outlet (a). The absence of electrons with negative velocities near the orifice outlet means that all the electrons that leave the E-K gap contribute to the anode current.

The system returns to its initial state, as shown in Fig. 8, when ions leave the K-A gap. The electric field accelerates ions up to velocity  $v_i = \sqrt{2e\Delta\phi/M}$ , so that the ions are removed from the K-A gap during the time  $t_i = 2d_{pl}/v_i$ , where  $\Delta\phi$  is the potential drop across the gap, and  $d_{pl}$  is the length of this gap. In the presented numerical simulation,  $\Delta\phi \approx 60$  V and  $d_{pl} = 0.37$  mm. Thus,  $t_i \approx 5.6$  ns, which agrees well with the simulation results (see Fig. 4).

Finally, the enhancement of the electron current extracted from the discharge plasma through the keeper orifice leads to an increase in the positive potential of this plasma with respect to the cathode. Because of the large difference between the plasma densities in the E-K and K-A gaps, this variation in the potential is small. Nevertheless, the variation in the emitted electron current density from the emitter caused by the Schottky effect is clearly visible in

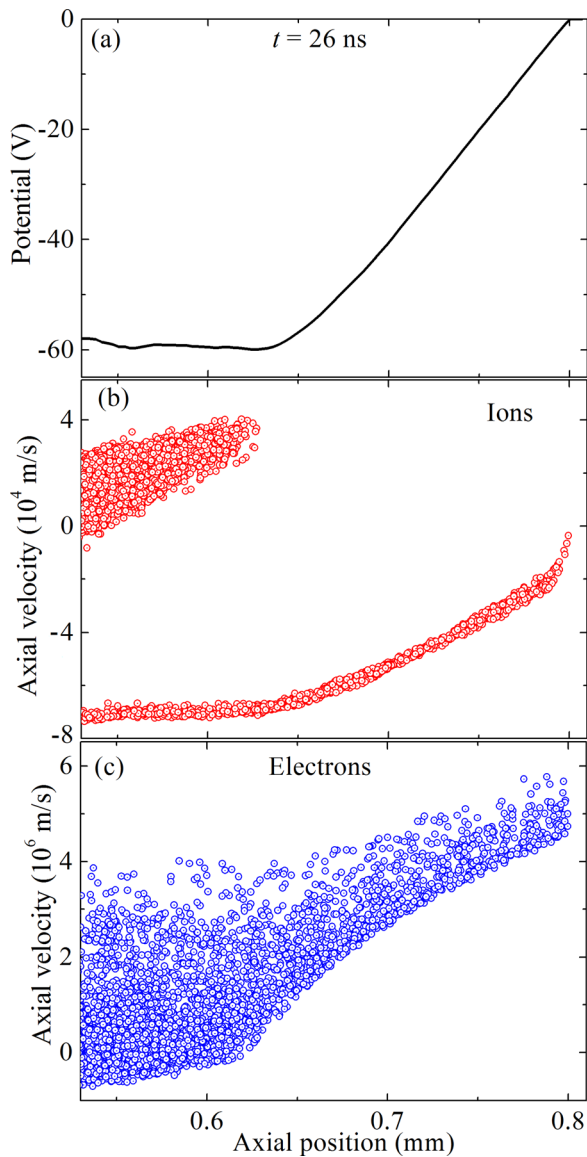


FIG. 8. Axial distribution of the potential  $\phi(z)$  (a) and phase space  $v_z(z)$  of ions (b) and electrons (c) at  $t = 20.4$  ns. Compare with Fig. 4.

Fig. 2. The smallness of the emitted current variation also confirms that processes in the K-A gap are responsible for the automodulation of the anode current.

### III. CONCLUSIONS

The evolution of the plasma plume created by the micro-hollow cathode discharge was studied using a 2D self-consistent particle-in-cell Monte Carlo collision simulation.

It was shown that two stages of the plasma plume dynamics can be distinguished. The first stage is characterized by the expansion toward the anode of the quasi-neutral plasma penetrating from the emitter-keeper gap through the keeper orifice into the keeper-anode gap. At this stage, the anode current is limited by electron space charge between the plume boundary and the anode (Child-Langmuir current). When the distance between the plume boundary and the anode becomes so small that the space-charge limited current exceeds the plasma thermal electron current through the small keeper orifice, the plasma quasi-neutrality is violated and the electric field penetrates the plasma plume bulk. During this second stage, the electric field removes plasma ions from the keeper-anode space. The process of plume formation and its expansion toward the anode is reiterated when ions leave the anode-keeper gap. The electron current extracted from the plasma experiences almost 100% periodic automodulation. Qualitative and quantitative estimations based on this two-stage model of plasma plume evolution are in good agreement with results of the numerical simulations.

<sup>1</sup>M. Keidar, T. Zhuang, A. Shashurin, G. Teel, D. Chiu, J. Lukas, S. Haque, and L. Brieda, *Plasma Phys. Controlled Fusion* **57**, 014005 (2015).

<sup>2</sup>D. Goebel and I. Katz, *Fundamentals of Electric Propulsion* (John Wiley & Sons, 2008).

<sup>3</sup>E. Oks, *Plasma Cathode Electron Sources* (Wiley-VCH, 2006).

<sup>4</sup>N. N. Koshelev and A. V. Loyan, in *30th International Electric Propulsion Conference, Florence, Italy, 17–20 September (2007)*, Paper No. IEPC-2007-103.

<sup>5</sup>V. Vekselman, Ya. E. Krasik, S. Gleizer, V. Tz. Gurovich, A. Warshavsky, and L. Rabinovich, *J. Propul. Power* **29**, 475 (2013).

<sup>6</sup>G. Xia, G. Mao, and N. Sadeghi, *Tsinghua Sci. Technol.* **14**, 49 (2009).

<sup>7</sup>P. Gessini, S. B. Gabriel, and D. G. Fearn, in *27th International Electric Propulsion Conference, Pasadena, CA, 15–19 October (2001)*, Paper No. IEPC-01-233.

<sup>8</sup>M. T. Domonkos, A. D. Gallimore, and M. J. Patterson, *J. Propul. Power* **19**, 438 (2003).

<sup>9</sup>I. G. Mikellides, I. Katz, D. M. Goebel, and K. K. Jameson, *J. Appl. Phys.* **101**, 063301 (2007).

<sup>10</sup>B. A. Jorns, I. G. Mikellides, and D. M. Goebel, *Phys. Rev. E* **90**, 063106 (2014).

<sup>11</sup>D. Levko, Ya. E. Krasik, V. Vekselman, and I. Haber, *Phys. Plasmas* **20**, 083512 (2013).

<sup>12</sup>D. Levko, Y. P. Bliokh, and Ya. E. Krasik, *Phys. Plasmas* **22**, 063503 (2015).

<sup>13</sup>J. P. Boeuf and L. Garrigues, *J. Appl. Phys.* **84**, 3541 (1998).

<sup>14</sup>V. K. Rawlin and E. V. Pawlik, "A mercury plasma-bridge neutralizer," AIAA Paper No. 67-670, 1967.

<sup>15</sup>D. P. Grote, A. Friedman, J. L. Vay, and I. Haber, *AIP Conf. Proc.* **749**, 55 (2005).

<sup>16</sup>K. P. Stanukovich, *Unsteady Flows of a Continuous Medium* (Nauka, Moscow, 1971).

<sup>17</sup>G. Jaffé, *Phys. Rev.* **65**, 91 (1944).